The spin–flip approach within time-dependent density functional theory: Theory and applications to diradicals

Yihan Shao and Martin Head-Gordon
Department of Chemistry, University of California, Berkeley, Berkeley, California 94720

Anna I. Krylov
Department of Chemistry, University of Southern California, Los Angeles, California 90089-0482

(Received 23 October 2002; accepted 19 December 2002)

An extension of density functional theory to situations with significant nondynamical correlation is presented. The method is based on the spin–flip (SF) approach which is capable of describing multireference wave functions within a single reference formalism as spin–flipping, e.g., $\alpha \rightarrow \beta$, excitations from a high-spin ($M_s=1$) triplet reference state. An implementation of the spin–flip approach within the Tamm–Dancoff approximation to time-dependent density functional theory (TDDFT) is presented. The new method, SF-TDDFT/TDA or simply SF-DFT, describes target states (i.e., closed- and open-shell singlets, as well as low-spin triplets) by linear response from a reference high-spin triplet ($M_s=1$) Kohn–Sham state. Contrary to traditional TDDFT, the SF-DFT response equations are solved in a subspace of spin–flipping operators. The method is applied to bond-breaking (ethylene torsional potential), and equilibrium properties of eight diradicals. The results demonstrate significant improvement over traditional Kohn–Sham DFT, particularly for 50/50 hybrid functional. © *2003 American Institute of Physics.* [DOI: 10.1063/1.1545679]

I. INTRODUCTION

Electronic degeneracy is ubiquitous in chemistry. For example, bonding and antibonding orbitals may become degenerate at a dissociation limit or transition state, degenerate frontier orbitals are common in diradicals and other open-shell intermediates. Orbital (near)-degeneracies result in wave functions which are not dominated by a single configuration, but rather include several leading determinants. Therefore, the Hartree–Fock description of such multiconfigurational wave functions is qualitatively incorrect. This often causes a breakdown of single-reference post-Hartree–Fock methods, e.g., Møller–Plesset (MP) and coupled-cluster (CC) methods.[1]

The traditional approach to these problems is a two-step procedure. First, a zero-order wave function which consists of a small number of near-degenerate configurations is calculated in order to recover nondynamical correlation. This can be done by the multiconfigurational self-consistent field (MCSCF) procedure,[2,3] most often implemented as complete active space SCF (CASSCF). Remaining effects, i.e., dynamical correlation, are then recovered by configuration interaction (MRCI), perturbation theory (MRPT), or MRCC (see Ref. 4 for a comprehensive review of multireference methods).

Recently, several single-reference methods capable of describing some multireference situations have been developed: the valence optimized-orbitals coupled-cluster doubles (VOO-CCD) method,[5–7] quadratic CCD (QCCD),[8,9] doubly ionized equation-of-motion CCSD,[10] and the spin–flip (SF) approach.[11–14] These single-reference methods are application-independent (in the sense that no specification of near-degenerate configurations or active orbitals is required), size-consistent, and relatively cost-effective. This work presents a new extension of the SF approach.

Within the SF approach,[11–14] a high-spin ($M_s=1$) triplet state with two unpaired α-electrons is chosen as a reference. Target $M_s=0$ states (both closed- and open-shell singlet states, and $M_s=0$ components of triplet states) are then described as a spin–flipping, e.g., $\alpha \rightarrow \beta$, excitation from the reference. In cases where large nondynamical correlation derives from a single HOMO-LUMO pair (e.g., bonding and antibonding orbitals in single-bond breaking reactions and homosymmetric diradicals, nonbonding orbitals in heterosymmetric diradicals[15]), the SF approach provides a more balanced description than the corresponding traditional single-reference methods which overemphasize the importance of the closed-shell Hartree–Fock configuration. Moreover, SF is a multistate approach and is therefore capable of describing several states in one calculation. For example, the SF models accurately describe all three low-lying singlet diradical states,[15] i.e., closed-shell singlet, open-shell singlet, and second closed-shell singlet which is a doubly-excited state with respect to the first closed-shell singlet.[13,14]

By employing theoretical models of increasing complexity for the reference wave function, the description of the final SF states can be systematically improved. The simplest member of the SF hierarchy of models is the SF configuration interaction singles method (SF-CIS) (Ref. 11) which employs the SCF wave function for the reference, and describes the final states as single excitations flipping the spin of one electron (e.g., where an α-electron is excited into a β virtual orbital). SF-CIS has been shown to give a reasonable account of the nondynamical correlation, thus extending the SCF/CIS models to bond-breaking and diradicals. Moreover, for excited states (e.g., singlet–triplet energy gaps in diradi-

cals) it represents a considerable improvement over CIS, its traditional spin-conserving counterpart. More accurate description is achieved by recovering more dynamical correlation through higher-order excitations by PT [SF-CIS(D)],[13] CI (SF-CISD),[12] or CC (SF-OO-CCD or SF-OD).[11]

Since target SF states can formally be considered as linear response states of the reference triplet state, the SF idea can be implemented within time-dependent density functional theory (TDDFT). Even though DFT (Refs. 16–18) and TDDFT (Refs. 19–25) are formally exact[16,19,20] practical implementations involve an unknown functional of the density, for which a number of models have been developed.[26–33] So far, the success of these functionals is limited to systems whose ground state electronic structure is dominated by a single Slater determinant. This can be related to the parameterization of the density by a fictitious Slater determinant (i.e., the Kohn–Sham determinant) in the Kohn–Sham equations.[17] Had the exact functional existed, this parameterization would yield the exact density for any (i.e., including multiconfigurational) wave function. With the available inexact functionals, however, the Kohn–Sham determinant not only represents the total density, but also reflects the leading electronic configuration in the many-electron wave function. It is therefore not surprising that such a description can fail for systems with strong multireference character.[34]

Despite the above limitation, DFT has become very popular for its ability to describe dynamical correlation[35–37] within a computationally inexpensive one-electron computational scheme. In many chemical applications, its accuracy is comparable to MP2 and sometimes even CCSD methods.[38] This success has motivated the development of several approaches for including nondynamical correlation within Kohn–Sham DFT.[34,37,39–54] Many of these techniques adhere to a single Kohn–Sham determinant representation of the electron density, e.g., the sum method;[39] restricted open shell theory for singlets (ROSS-DFT);[34,40] ensemble theory;[41–43] and the fractional occupation number (FON) method.[44–46] Alternatively, one can employ a wave-function-like approach, and use several Kohn–Sham determinants for the parameterization.[34,37,47–54] These determinants can be chosen by using multireference techniques, such as valence-bond, MCSCF, or VOO-CCD. Thus, these hybrid methods combine DFT (to simulate dynamical correlation) with the multireference models (to treat nondynamical correlation). Unfortunately, a multi-determinantal parameterization will generally make these methods significantly more expensive. Moreover, the possible double counting of electronic correlation must be accounted for.[34,50,51] Nevertheless, the ability of wave function based methods to extend DFT suggests it is worthwhile to explore the SF approach to describe nondynamical correlation within the single-determinantal Kohn–Sham scheme.

The merge of the SF approach with DFT proceeds through TDDFT,[19–25] a formally exact single-excitation theory based on Kohn–Sham orbitals. TDDFT describes excited states as a linear response of the ground state density. When implemented within the Tamm–Dancoff approximation (TDA),[55] the resulting equations are isomorphic to the CIS equations (with properly redefined Coulomb and exchange integrals),[24,25] which greatly simplifies the implementation. Although invoking the TDA within TDDFT yields a formally inexact theory, it has been shown that the TDA does not considerably affect excitation energies in most cases.[24,25] Moreover, the TDA sometimes yields improved results over full TDDFT,[22,25] although this surely results from cancellation of errors.

TDDFT has been shown to yield more accurate results than CIS,[24,25] including valence excited states with considerable doubly excited character for which CIS fails dramatically.[24] However, the TDDFT description of Rydberg states (or diffuse valence states) is rather poor due to the incorrect asymptotic behavior of the available functionals (see, for example, Ref. 56). As far as bond-breaking is concerned, TDDFT inherits all the limitations of ground-state DFT. Therefore, a combination of the SF approach with TDDFT can be a simple tool to recover both nondynamical (from SF) and dynamical (from DFT) correlation. The attractive feature of this approach is that it is based on formally exact response theory, and, therefore, SF-TDDFT will yield exact results (also identical to non-SF DFT) if the (yet unknown) exact functional of the density is used. In this paper, we present this method in the Tamm–Dancoff approximation (SF-TDDFT/TDA, or simply SF-DFT) and investigate its performance. We choose to invoke TDA because of the simplifications it offers, although SF-TDDFT/TDA is an approximation to the full SF-TDDFT theory.

The paper is organized as follows: in the next section, we present the working equations for SF-DFT. Section III presents the results for twisted ethylene and selected diradicals. Our concluding remarks are given in Sec. IV.

II. THE METHOD

In Kohn–Sham DFT, the electron density $\rho(x)$ is expanded over a set of M one-electron (real-valued) orthonormal basis functions $\{\phi_p(x)\}_{p=1}^{M}$:

$$\rho(x)=\sum_{pq}^{M}\mathbf{P}_{pq}\phi_p(x)\phi_q(x), \tag{1}$$

where x denotes spatial and spin coordinates of an electron, $x=(r,\sigma)$, and the density matrix $\mathbf{P}$ is subject to idempotency and normalization conditions:

$$\mathbf{P}^2=\mathbf{P}, \tag{2}$$

$$\mathrm{tr}[\mathbf{P}]=N, \tag{3}$$

where N is a total number of electrons.

In TDDFT, the time-evolution of the reference state density matrix follows the time-dependent Kohn–Sham equation:

$$[\mathbf{F}+\lambda\mathbf{V}(t),\mathbf{P}]=i\frac{\partial\mathbf{P}}{\partial t}, \tag{4}$$

where $\lambda\mathbf{V}(t)$ is an infinitesimal oscillatory perturbation, and $\mathbf{F}$ is the Kohn–Sham Hamiltonian matrix,[57] which consists

of the fictitious one-electron kinetic energy, nuclei–electron attraction, electron–electron Coulomb repulsion, and the exchange-correlation potential $\hat{v}_{\mathrm{xc}}$:

$$\mathbf{F}_{pq}=\int \phi_p(x)\left[-\frac{1}{2}\nabla_r^2-\sum_A \frac{Z_A}{|r-R_a|} + \int \frac{\rho(x')dx'}{|r-r'|}+\hat{v}_{\mathrm{xc}}(x)\right]\phi_q(x)dx. \tag{5}$$

By applying time-dependent perturbation theory to Eq. (4), the time-independent Kohn–Sham equation for the reference state density matrix is retrieved in the zero-order:

$$[\mathbf{F}^{(0)},\mathbf{P}^{(0)}]=0, \tag{6}$$

$$\mathbf{F}^{(0)}_{pq}=\delta_{pq}\epsilon_p, \tag{7}$$

$$\mathbf{P}^{(0)}_{ij}=\delta_{ij}, \tag{8}$$

$$\mathbf{P}^{(0)}_{ia}=\mathbf{P}^{(0)}_{ai}=\mathbf{P}^{(0)}_{ab}=0, \tag{9}$$

where ϵ_p denotes the Kohn–Sham orbital energies, indexes $i,j,\ldots$ are reserved for the spin–orbitals which are occupied in the reference Kohn–Sham determinant, indexes $a,b,\ldots$ are used for the unoccupied spin–orbitals, and indexes $p,q,\ldots$ denote spin–orbitals which can be either occupied or unoccupied in the reference.

Conditions that define the Bohr frequencies (excitation energies) from the reference ground state are obtained from the poles of the linear response (i.e., in the first order) of the reference state density matrix:[21–24]

$$\begin{pmatrix}\mathbf{A} & \mathbf{B}\\ \mathbf{B}^* & \mathbf{A}^*\end{pmatrix}\begin{pmatrix}\mathbf{X}\\ \mathbf{Y}\end{pmatrix}=\omega\begin{pmatrix}\mathbf{1} & \mathbf{0}\\ \mathbf{0} & -\mathbf{1}\end{pmatrix}\begin{pmatrix}\mathbf{X}\\ \mathbf{Y}\end{pmatrix}, \tag{10}$$

$$\mathbf{A}_{ia,jb}=(\epsilon_a-\epsilon_i)\delta_{ab}\delta_{ij}+\frac{\partial \mathbf{F}_{ia}}{\partial \mathbf{P}_{jb}}, \tag{11}$$

$$\mathbf{B}_{ai,bj}=\frac{\partial \mathbf{F}_{ai}}{\partial \mathbf{P}_{jb}}. \tag{12}$$

Within the TDA, one obtains[25]

$$\mathbf{A}\mathbf{X}^I=\omega_I\mathbf{X}^I, \tag{13}$$

where ω_I denotes an excitation energy to the Ith excited state, whose density can be calculated from the corresponding response matrix $\mathbf{X}^I$ as follows:

$$\mathbf{P}^I_{ij}=\delta_{ij}-\sum_a \mathbf{X}^I_{ia}\mathbf{X}^I_{ja}, \quad \mathbf{P}^I_{ab}=\sum_i \mathbf{X}^I_{ia}\mathbf{X}^I_{ib}. \tag{14}$$

The above equation allows one to interpret an electron excitation in terms of changes in populations of the Kohn–Sham orbitals. Likewise, Eqs. (13) and (11) show that there are two different contributions to the excitation energy ω_I: the energy difference between the Kohn–Sham orbitals whose populations change upon the excitation (this would be an exact excitation energy for noninteracting electrons), and the correlation part which is folded into the dependence of the Fock matrix on the density matrix.

In the traditional TDDFT implementations,[24,25] only spin-conserving blocks, i.e., $\alpha\alpha$ and $\beta\beta$, of the response matrix $\mathbf{X}$ are allowed to be nonzero. In this case, number of α and β electrons does not change upon excitation. In the SF implementation, we consider only $\alpha\beta$ blocks of $\mathbf{X}$, which results in a net change of α and β electrons upon excitation (one α-electron is promoted to the empty β-orbital). In the subsequent section, we discuss contributions into the $\alpha\beta,\alpha\beta$ block of the coupling matrix $\mathbf{A}$ from Eqs. (13) and (11).

A. Contributions to the coupling matrix

Similarly to the non-SF case, the diagonal part of the matrix $\mathbf{A}$ is simply differences between energies of α-occupied and β-virtual Kohn–Sham orbitals. In case of noninteracting electrons, these differences give exact excitation energies. The correlation effects are described by the dependence of the effective one-particle Hamiltonian on the electron density. This dependence couples different one-electron excitations. Below we discuss the contributions to the SF block of $\partial\mathbf{F}/\partial\mathbf{P}$ by analyzing how different parts of the Fock matrix from Eq. (5) depend upon the density matrix $\mathbf{P}$. Note that the Fock matrix (5) which appears in the excited state equations [Eqs. (13) and (11)] depends upon the *reference state's density*.

The first two terms in Eq. (5), i.e., the one-electron kinetic energy and nuclear–electron attraction, do not depend on the density matrix, and therefore they do not contribute to the coupling part of $\mathbf{A}$. The third term, the Coulomb operator, is represented in matrix form as

$$\begin{aligned}\mathbf{J}_{pq}&=\int \phi_p(x)\left[\int dx'\frac{\rho(x')}{|r-r'|}\right]\phi_q(x)dx\\ &=\int \phi_p(x)\left[\int dx'\frac{\sum_{st}\mathbf{P}_{st}\phi_s(x')\phi_t(x')}{|r-r'|}\right]\phi_q(x)dx\\ &=\sum_{st}\int\int dxdx'\,\phi_p(x)\phi_t(x')\frac{1}{|r-r'|}\phi_q(x)\phi_s(x')\mathbf{P}_{st}\\ &=\sum_{st}\langle pt|qs\rangle\mathbf{P}_{st}\end{aligned} \tag{15}$$

and the corresponding derivative is

$$\frac{\partial \mathbf{J}_{ia}}{\partial \mathbf{P}_{jb}}=\langle ib|aj\rangle. \tag{16}$$

It vanishes for spin–flipping excitations because in the 2-electron repulsion integral $\langle ib|aj\rangle$ two spin–orbitals for the first electron have opposite spin: a has β-spin while i has α-spin. Similarly, the two spin–orbitals of the second electron also have opposite spin. Therefore, the Coulomb potential *does not* couple different spin–flipping single electron excitations. This is hardly surprising, since neither the α-electron nor the β-electron reference state density are affected by changes in the $\beta\alpha$ block of the density matrix.

The exchange-correlation potential from Eq. (5) can be parameterized as follows:[32]

$$\hat{v}_{\mathrm{xc}}(x)=c_1\hat{v}_x(r)+c_2\hat{v}_c(r)+c_3\hat{v}_x^{\mathrm{HF}}(x), \tag{17}$$

where the first two terms represent exchange and correlation potentials, respectively, and the last term is the Hartree–Fock (or exact) exchange:

$$\hat{v}_x^{\mathrm{HF}}(x) = -\int dx' \frac{\rho(x,x')}{|r-r'|}\hat{P}_{x,x'}, \tag{18}$$

where $\hat{P}_{x,x'}$ is a permutation operator. Just like the Coulomb potential, pure exchange or correlation potentials depend only on α- or β-electron densities and their gradients, and therefore they do not couple single electron SF excitations.

The Hartree–Fock exchange, however, involves off-diagonal elements of the density matrix which can be affected by $\alpha\beta$-block changes in the density matrix,

$$\begin{aligned}\mathbf{K}_{pq} &= -\int \phi_p(x)\left[\int dx' \frac{\rho(x,x')}{|r-r'|}\hat{P}_{x,x'}\right]\phi_q(x)dx \\ &= -\int dx\,\phi_p(x)\int dx' \frac{\sum_{st}\mathbf{P}_{st}\phi_s(x)\phi_t(x')}{|r-r'|}\phi_q(x') \\ &= -\sum_{st}\int\int dx dx'\,\phi_p(x)\phi_t(x')\frac{1}{|r-r'|}\phi_s(x)\phi_q(x')\mathbf{P}_{st} \\ &= -\sum_{st}\langle pt|sq\rangle \mathbf{P}_{st}. \end{aligned} \tag{19}$$

The derivative is given by

$$\frac{\partial \mathbf{K}_{ia}}{\partial \mathbf{P}_{jb}} = -\langle ib|ja\rangle \tag{20}$$

and is indeed nonvanishing for the SF excitations. Thus, *only the Hartree–Fock exchange contributes to the SF coupling block of the matrix* **A**.

B. Implementation and computational details

We have implemented the SF-DFT method in the Q-CHEM *ab initio* package.[58] This implementation is direct,[58] meaning that no two-electron integrals are stored. Furthermore, all operations involving two-electron integrals are performed in the atomic orbital basis. Practically, a SF-DFT calculation with a pure exchange functional (i.e., containing no HF exchange) is trivial in the sense that the excitation energies are simply the orbital energy differences between α-occupied and β-virtual Kohn–Sham orbitals. The SF-DFT implementation with a hybrid exchange functional [such as B3 (Ref. 32) is similar to a SF-CIS calculation, the main difference being that the Hartree–Fock exchange contribution from Eq. (20) needs to be weighted in SF-DFT.

In our calculations, we use three exchange-correlation functionals: (i) BLYP;[29,30] (ii) B3LYP (Ref. 32) [20% Hartree–Fock+8% Slater[26]+72% Becke[29] for exchange and 19% VWN (Ref. 27)+81% LYP (Ref. 30) for correlation]; and (iii) the 50/50 functional (50% Hartree–Fock+8% Slater +42% Becke for exchange and 19% VWN+81% LYP for correlation) which includes a larger fraction of the Hartree–Fock exchange relative to B3LYP. We shall denote calculations with these functionals as SF-BLYP, SF-B3LYP, and SF-5050, respectively.

Note that there is an interesting connection between SF-DFT and the DFT/MRCI method of Grimme and Waletzke.[53] They employ KS theory to obtain orbitals and orbital energies, and then perform truncated CI calculations with screened integrals. The method of Grimme and Waletzke[53] becomes equivalent to the SF-5050 model if the SF procedure of generating the CI determinantal space and the screening parameter of 0.5 are used within their DFT/MRCI scheme.

In the next section, we discuss two chemically important situations where currently available DFT models fail: bond-breaking (ethylene torsional potential) and diradicals (equilibrium properties and singlet–triplet gaps). For ethylene, we have employed a DZP basis set which is the standard Huzinaga–Dunning DZ basis[59] augmented by six *d*-type functions with the exponent 0.75 for carbons and by three *p*-type functions with the exponent 0.75 for hydrogens. The diradicals have been studied with the 6-31G* basis set.[60] The optimized geometries and total energies for diradicals' triplet states have been calculated by using the $M_s=0$ SF states rather than the $M_s=1$ reference states. In all the SF calculations, spin-unrestricted triplet references have been used. Adiabatic energy separations have been calculated as differences between total energies calculated at the geometries optimized at the same level of theory as used for the energy calculation.

III. RESULTS AND DISCUSSIONS

A. Ethylene torsion

Ethylene's torsional potential is a classical example of nondynamical correlation. At equilibrium, the π and π^* orbitals are well separated in energy, and the Hartree–Fock determinant, $(\pi)^2$, is a qualitatively correct wave function. However, at 90°, the π and π^* orbitals become degenerate, causing a breakdown of standard spin-restricted single-reference methods. Thus, in order to accurately describe the torsional potential, the wave function should include both $(\pi)^2$ and $(\pi^*)^2$ configurations. Moreover, qualitatively correct wave functions should be flexible enough to treat these configuration on an equal footing. This can be achieved, for example, by two-configurational SCF (TCSCF) augmented by configuration interaction including single and double excitations (TC-CISD). Below, we use TC–CISD curve[13] as the reference. The $\pi-\pi^*$ degeneracy does not affect the $\pi\alpha\pi^*\alpha$ triplet state, which is well described by a single determinant at all torsional angles. Since both $(\pi)^2$ and $(\pi^*)^2$ determinants are single spin–flipping excitations from the $\pi\alpha\pi^*\alpha$ triplet, the SF model can accurately describe the ground-state state wave-function at all torsional angles (see Refs. 11–14).

Potential energy curves along the torsional coordinate calculated by spin-restricted HF and DFT (using BLYP, B3LYP, and 5050 functionals) methods are shown in Fig. 1. Since the second important determinant, $(\pi^*)^2$, is completely neglected by the Hartree–Fock model, RHF produces a potential curve with an unphysical cusp and overestimates

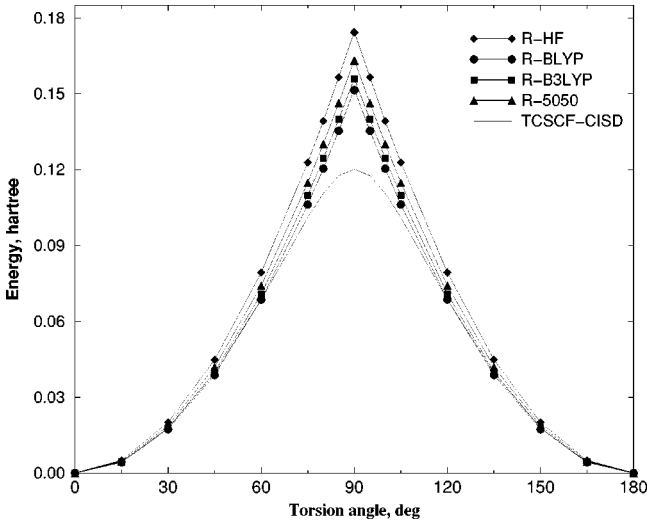

FIG. 1. Ethylene torsional potential, DZP basis. All curves are shifted such that the energy at 0° is zero. Spin-restricted Hartree–Fock and DFT curves display a sharp cusp around the barrier. The barrier height is considerably overestimated.

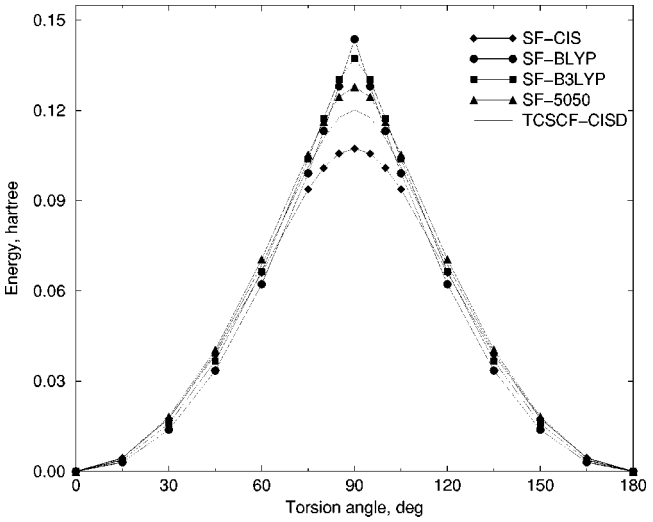

FIG. 3. Ethylene torsional potential, DZP basis. All curves are shifted such that the energy at 0° is zero. All SF curves (except for the SF-BLYP one) are smooth.

the barrier height by about 1.5 eV. Spin-restricted DFT curves are qualitatively and quantitatively similar to the RHF one.

The spin-unrestricted HF method yields a smooth curve, but at the price of spin-contamination: at the barrier, $\langle S^2 \rangle \approx 1$ which corresponds to an even mixture of singlet and triplet states. Moreover, the barrier height and the shape of the unrestricted curve is not very accurate: UHF underestimates the barrier height by 1.1 eV (the RHF error is 1.5 eV). The heavy spin-contamination is not rectified by using correlated wave functions.[61] Likewise, correlated models which use UHF references yield only marginally more accurate energies than their RHF-based counterparts.[61]

Figure 2 shows spin-unrestricted curves calculated by the UHF, U-BLYP, U-B3LYP, and U-5050 models. The spin-symmetry breaking improves DFT curves much more drastically than the wave function based models,[61] for example, U-B3LYP underestimates the barrier height by only 0.25 eV. Nevertheless, the heavy spin-contamination and difficulties associated with finding an appropriate spin-symmetry broken solution are discouraging as far as practical use of U-DFT is concerned.

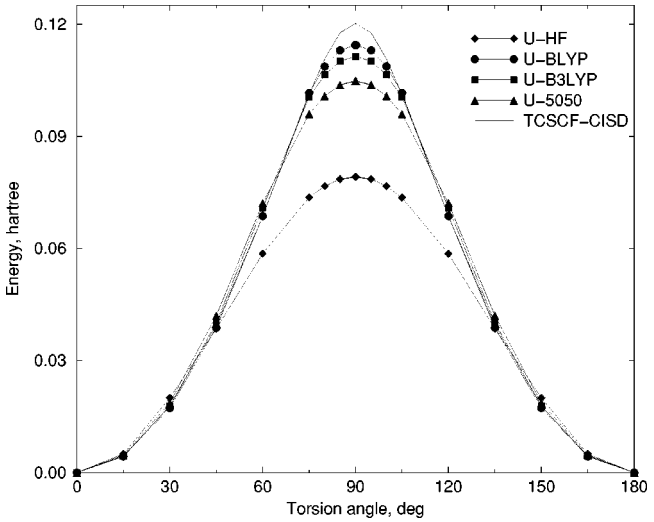

FIG. 2. Ethylene torsional potential, DZP basis. All curves are shifted such that the energy at 0° is zero. Spin-unrestricted Hartree–Fock and DFT methods yield smooth curves, at the price of spin-contamination. Moreover, barrier height is underestimated.

Potential energy curves calculated by the SF-CIS, SF-BLYP, SF-B3LYP, and SF-5050 methods are shown in Fig. 3. SF-CIS, SF-B3LYP, and SF-5050 curves are all smooth around the barrier. In contrast, the SF-BLYP curve has a cusp, due to the fact there is no coupling between different excitations in pure exchange-correlation functionals (see Sec. II A). The residual spin-contamination is very small for all the methods: the $\langle S^2 \rangle$ values are less than 0.1. The SF-5050 barrier height is less than 0.2 eV from the reference TC-CISD value.

Selected total energies from Figs. 1–3 are given in Table I. Table II presents the optimized geometries and barrier heights. As far as optimized barrier heights are concerned, SF-CIS underestimates the barrier by 0.32 eV, SF-B3LYP overestimates the barrier by 0.65 eV (as compared with the more accurate SF-OD model). The SF-5050 optimized barrier height is 3.15 eV, which is 0.35 eV higher than the SF-OD value.

B. Diradicals

As defined by Salem, diradicals are molecules with two electrons occupying two (near)-degenerate molecular orbitals.[15] While diradicals are essential in interpreting reaction mechanisms,[62–65] their theoretical treatment is difficult due to the multiconfigurational character of their singlet wave functions. Their high-spin triplet states, however, are single-configurational—just like the triplet $\pi\pi^*$ state in the twisted ethylene example. As has been demonstrated in the recent benchmark study,[14] the SF approach accurately describes low-lying diradicals' singlet states as spin–flipping

TABLE I. Ethylene torsion, DZP basis. Total energies, hartree, for the SF-BLYP, SF-B3LYP, and SF-5050 models. Unoptimized barrier height, $\Delta E = E(90°) - E(0°)$, is also shown.[a] Geometry used: $r_{CC} = 1.330$ Å, $r_{CH} = 1.076$ Å, $\alpha_{HCH} = 116.6°$.

Angle (deg)	SF-BLYP	SF-B3LYP	SF-5050
0	−78.506 23	−78.570 70	−78.534 17
15	−78.503 11	−78.566 87	−78.529 57
30	−78.492 36	−78.554 82	−78.515 96
45	−78.472 66	−78.533 90	−78.493 69
60	−78.444 05	−78.504 25	−78.463 65
75	−78.407 09	−78.466 89	−78.428 82
80	−78.393 05	−78.453 34	−78.417 99
85	−78.378 21	−78.440 47	−78.409 65
87	−78.372 05	−78.436 34	−78.407 58
89	−78.365 78	−78.433 81	−78.406 49
90	−78.362 57	−78.433 44	−78.406 34
ΔE	3.91	3.74	3.48

[a]SF-CIS torsional potentials can be found in Ref. 11, the corresponding unoptimized barrier height is 2.92 eV. The unoptimized TC-CISD and SF-OD barriers are 3.27 and 3.23 eV, respectively (Ref. 13). The corresponding values (in eV) for the traditional HF and DFT calculations are: 4.76 and 2.15 eV (RHF/UHF) (Ref. 61), 4.12 and 3.11 (R-BLYP and U-BLYP), 4.24 and 3.03 (R-B3LYP and U-B3LYP), 4.44 and 2.85 (R-5050 and U-5050).

excitations from the high-spin triplet reference (which sometimes happens to be a diradical's ground state, such as in methylene or trimethylenemethane).

In this work, we investigate the performance of SF-DFT for (i) equilibrium structures and frequencies of singlet diradicals; and (ii) energy gaps between the lowest singlet and triplet states (this is a chemically important question, because the reactivity of singlet and triplet diradicals is often considerably different[66]). We have selected the following eight moderate-size diradicals as our benchmark set: *ortho*-benzyne (**1**), *meta*-benzyne (**2**), *para*-benzyne (**3**), *m*-benzoquinodimethane (*m*-xylylene, C_8H_8, **4**), propane-1,3-diyl (C_3H_6, **5**), 2,2-difluoropropane-1,3-diyl ($C_3H_4F_2$, **6**), cyclopentane-1,3-diyl (C_5H_8, **7**), and 2,2-difluorocyclopentane-1,3-diyl (C_5H_8, **8**).

TABLE II. Optimized geometries for ethylene at the equilibrium (D_{2h}) and at the barrier (D_{2d}), DZP basis. Total energies and barrier height are also given.

Method	R_{CC}, Å	R_{CH}, Å	∠HCH	E_{tot}, hartree	ΔE, eV
Planar (D_{2h})					
SF-CIS[a]	1.352	1.077	117.1	−78.069 24	
SF-5050	1.335	1.080	116.9	−78.534 24	
SF-B3LYP	1.339	1.088	116.8	−78.571 20	
SF-CIS(D)[a]	1.345	1.084	116.9	−78.346 81	
SF-OD [a]	1.351	1.088	117.1	−78.389 29	
Twisted (D_{2d})					
SF-CIS[a]	1.472	1.080	117.3	−77.978 17	2.48
SF-5050	1.450	1.083	116.7	−78.418 37	3.15
SF-B3LYP	1.437	1.095	115.4	−78.444 36	3.45
SF-CIS(D)[a]	1.463	1.088	116.8	−78.244 01	2.80
SF-OD[a]	1.470	1.092	116.8	−78.286 26	2.80

[a]Reference 13.

Figures 4–7 show SF-DFT optimized geometries of the above diradicals in their lowest triplet and singlet states. Geometries calculated by the restricted and unrestricted HF and DFT models are not shown. Table III presents the corresponding adiabatic singlet–triplet energy gaps calculated by unrestricted HF and DFT (UHF, U-B3LYP, U-5050), and by the SF models (SF-CIS, SF-B3LYP, and SF-5050). Table III also presents experimental results[67,68] and best available theoretical estimates.[14,69–72]

Being the simplest σ-π aromatic diradicals, benzyne isomers (Fig. 4) have attracted considerable theoretical attention.[14,34,42,43,73–87] Additional interest in *p*-benzyne (**3**) originates in its role as an antitumor agent.[88] The ground state of all the three isomers is a singlet, and the lowest excited state is a triplet. The diradical character increases as the distance between the unpaired electrons increases in the *ortho*-→ *meta*-→ *para*- sequence. The increase in diradical character results in a singlet–triplet energy gap decrease in the same order: as determined in ultraviolet photoelectron spectroscopy experiments of Wenthold *et al.*,[67] ΔE_{st} are 35.5 ±0.3, 21.0±0.3, and 3.8±0.3 kcal/mol, respectively. As shown in Table III, RHF reverses the state ordering in all the three isomers. Restricted DFT models yield correct state ordering in *ortho*- and *meta*-isomers, however, the errors in the corresponding ΔE_{st} are quite large, e.g., R-B3LYP results are off by 8 and 5 kcal/mol for *o*- and *m*-C_6H_4, respectively. Moreover, both R-5050 and R-B3LYP fail dramatically for the most problematic *p*-benzyne. Errors in the spin-restricted methods are rather systematic: both RHF and R-DFT place the triplet too low with respect to the singlet, the imbalance increasing with the increase in the diradical character in this sequence. Spin-unrestricted results for these three diradicals are much less systematic. In *o*-benzyne, UHF yields correct state ordering, however, ΔE_{st} is off by 16 kcal/mol. U-5050 places the singlet too low with respect to the triplet. No instabilities have been found for the B3LYP model. In *m*-benzyne, only the Hartree–Fock model exhibits instabilities, however, the singlet's stabilization due to the spin-contamination is not sufficient to yield the correct state ordering. No instabilities for the DFT models have been found at the corresponding equilibrium geometries. There are, however, lower-energy spin-symmetry broken solutions at the triplet's equilibrium geometries, but the total energies of these solutions at their optimized geometries are higher than total energies of restricted solutions at their minima. This is because restricted models yield structures with the unphysically short distance between two radical centers (see, for example, Ref. 67). In *p*-benzyne, all unrestricted models yield the correct state ordering, however, UHF again overstabilizes the singlet. The SF-CIS method predicts correct multiplicity of the ground state for all three isomers. The SF-5050 results are in quantitative agreement with the experiment: errors do not exceed 4 kcal/mol.

Our next system, *m*-benzoquinodimethane (**4**, Fig. 5), is an example of a non-Kekulé molecule. EPR studies[68] have suggested a triplet ground state for this molecule, which has been confirmed by the TCSCF/STO-3G calculations.[69] For this molecule, the SF models predict the triplet state to be 7–10 kcal/mol below the singlet. Similarly to the previous

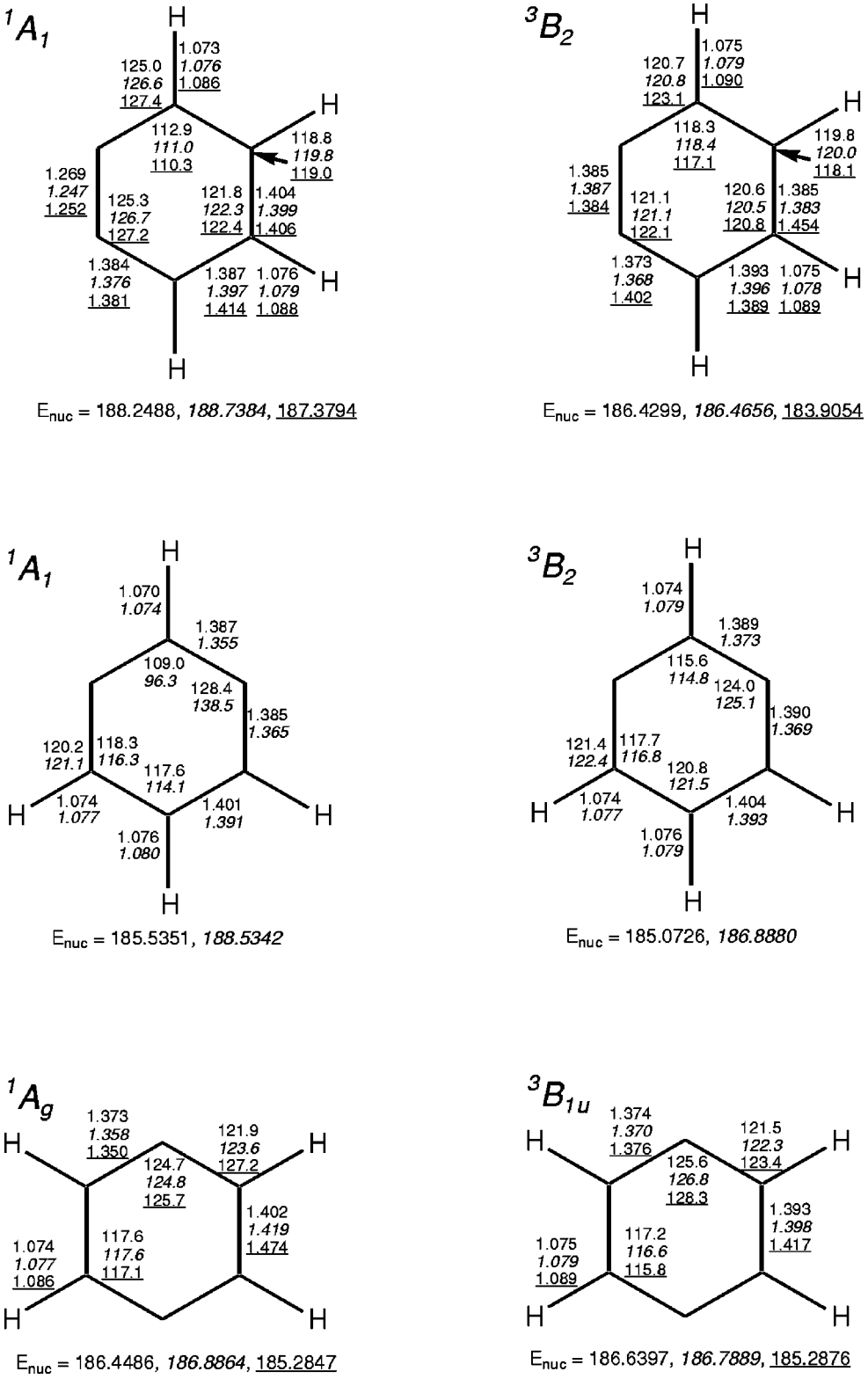

FIG. 4. Optimized geometries for the singlet and triplet states of benzynes (bond lengths are in angstroms, angles in degrees, and nuclear repulsion energies in hartrees) using SF-CIS (normal), SF-5050 (italic), and SF-B3LYP (underline) methods.

example, restricted models place the triplet state too low in energy with respect to the singlet which results in the grossly overestimated ΔE_{st}. Spin-symmetry breaking improves the results.

The next pair of molecules (Fig. 6), propane-1,3-diyl (**5**) and 2,2-difluopropane-1,3-diyl (**6**), are an interesting example, because the multiplicity of the ground state changes upon fluorination: the former diradical has a triplet ground state, and the latter has a singlet ground state.[42,70] CASPT2/6-31G* calculations[70] have predicted ΔE_{st} be -0.7 kcal/mol and 4.8 kcal/mol in (**5**) and (**6**), respectively. Restricted HF and DFT fail to describe this change: in both cases, triplet

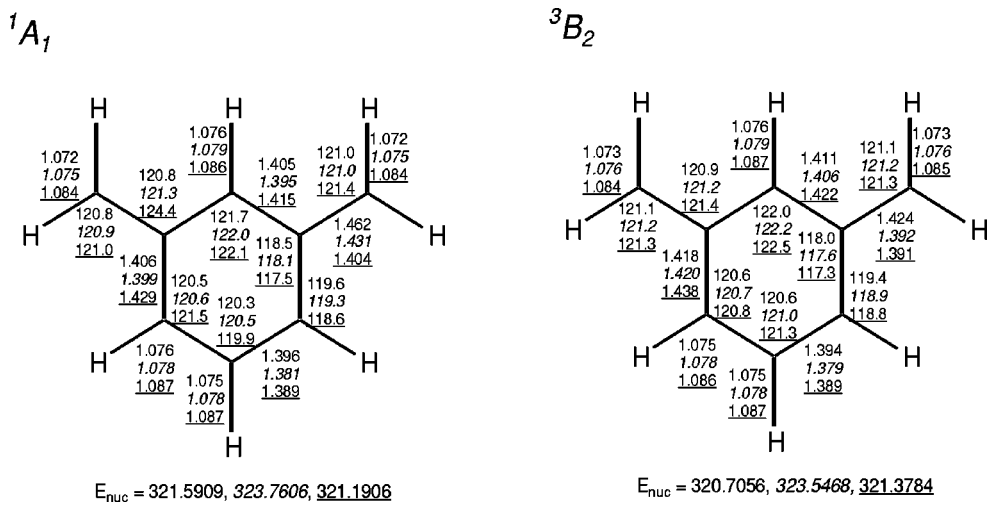

FIG. 5. Optimized geometries for the singlet and triplet states of *m*-benzoquinodimethane (bond lengths are in angstroms, angles in degrees, and nuclear repulsion energies in hartree) using SF-CIS (normal), SF-5050 (italic), and SF-B3LYP (underline) methods.

state is placed 10–80 kcal/mol below the singlet. Spin-unrestricted HF and DFT yield qualitatively correct results, however, the changes between the two systems seem to be underestimated by these methods (as compared with the CASPT2 results). Both the SF-CIS and the SF-5050 results are in quantitative agreement with CASPT2.

Similarly to (**5**) and (**6**), fluorine substitution reverses the state ordering in Closs's diradical (Fig. 7). Cyclopentane-1,3-diyl (**7**) has a triplet ground state as determined in the ESR and CISNP experiments,[89,90] and confirmed by the CISD calculations of Sherrill *et al.*[71] who have reported ΔE_{st} be -1.35 kcal/mol. The corresponding fluorinated molecule, 2,2-difluorocyclopentane-1,3-diyl (**8**), has a singlet ground state 9.8 kcal/mol below the lowest triplet (as determined by the CASPT2 calculations[72]). The performance of the restricted and unrestricted HF and DFT models is very similar to the previous example. The SF-CIS results are qualitatively correct, while SF-5050 is in quantitative agreement with CASPT2.

To summarize, the SF-CIS has been found to yield qualitatively correct results in all eight diradicals. The most accurate results are obtained by the SF-5050 method; the corre-

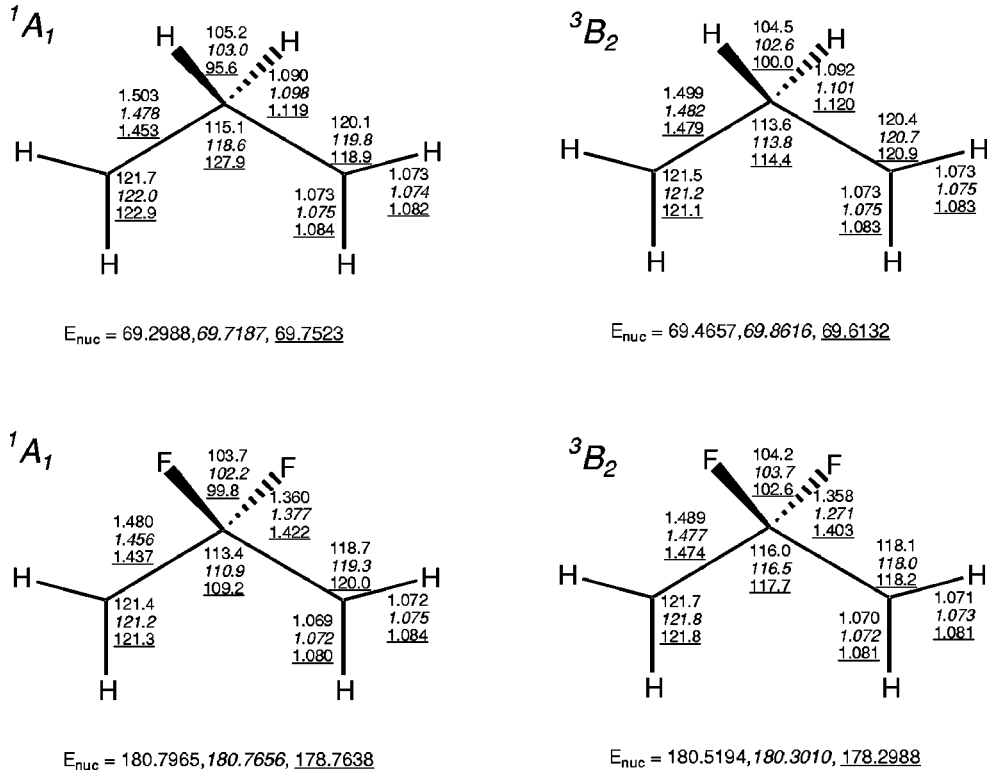

FIG. 6. Optimized geometries for the singlet and triplet states of propane-1,3-diyl and 2,2-difluopropane-1,3-diyl (bond lengths are in angstroms, angles in degrees, and nuclear repulsion energies in hartree) using SF-CIS (normal), SF-5050 (italic), and SF-B3LYP (underline) methods.

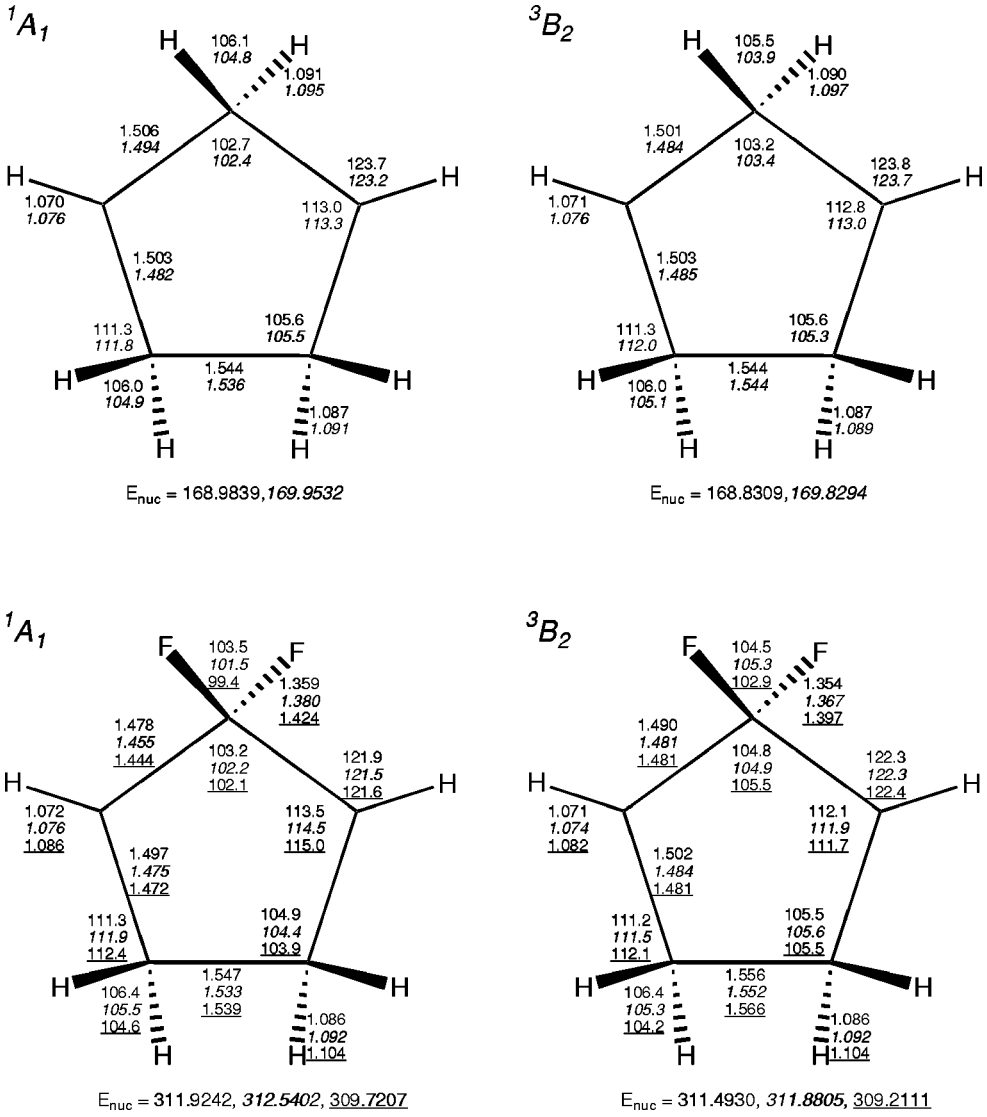

FIG. 7. Optimized geometries for the singlet and triplet states of cyclopentane-1,3-diyl and 2,2-difluorocyclopentane-1,3-diyl (bond lengths are in angstroms, angles in degrees, and nuclear repulsion energies in hartree) using SF-CIS (normal), SF-5050 (italic), and SF-B3LYP (underline) methods.

sponding ΔE_{st} are within 4 kcal/mol from the experimental or *ab initio* values. Spin-restricted models yield large errors: they systematically place triplet state too low with respect to the singlet state. Therefore, for diradicals with a singlet ground state, the ST gaps calculated by RHF and RDFT are either too small, or state ordering is reversed. For molecules with a triplet ground state, the ST gaps are grossly overestimated. Reference 14 explains the reasons for these systematic errors. Spin-unrestricted methods often (but not always, e.g., *m*-benzyne) improve the results, however, they often overstabilize singlets. The SF model provides systematic improvement over the spin-restricted and spin-unrestricted HF and DFT. Moreover, SF-CIS and SF-DFT are multistate methods and are capable of describing higher singlet states (see, for example, Ref. 14 which presents SF-CIS and SF-DFT results for the higher excited singlet states of trimethylenemethane diradical).

While SF-5050 gives a good account of the singlet–triplet gap for these medium-size radicals, it should be pointed out that SF-DFT apparently fails for small diradicals. For example, SF-5050 and SF-B3LYP reverse state ordering in CH_2, and yield too small singlet–triplet gaps in the C, O, Si atoms, and in NH, NF, and O_2. The reason why SF-DFT fails for smaller molecules while it succeeds quite well for the larger species is not clear to us.

In addition to equilibrium structures and adiabatic energy gaps, we also investigate how accurately the SF models reproduce shapes of potential energy surface. For this purpose, we consider vibrational frequencies of *p*-benzyne, a challenging test case for the *ab initio* methods. At the equilibrium geometry of this molecule, spin-restricted methods such as RHF, R-MP2, R-CCSD(T), suffer from orbital instabilities and fail to reproduce experimental vibrational spectrum even qualitatively correct; for example, they yield two large imaginary frequencies.[76,91] Spin-unrestricted methods have been more successful; U-CCSD(T) frequencies are in reasonable agreement with experiment.[76] Table IV presents calculated harmonic vibrational frequencies for the singlet ^1A_g ground state of *p*-benzyne as obtained by the SF-5050 and SF-B3LYP methods with a 6-31G** basis set. Experi-

TABLE III. Adiabatic singlet–triplet energy gaps (kcal/mol) calculated by the restricted and unrestricted HF, B3LYP, 5050, and the SF-CIS, SF-B3LYP, SF-5050 methods in a 6-31G* basis set. Zero-point energy corrections are not included into the theoretical results.

	o-C_6H_4 **1**	*m*-C_6H_4 **2**	*p*-C_6H_4 **3**	C_8H_8 **4**	C_3H_6 **5**	$C_3H_4F_2$ **6**	C_5H_8 **7**	$C_5H_6F_2$ **8**
RHF	−6.4	−29.1	−83.5	−88.4	−84.2	−63.3	−81.9	−49.5
R-5050	21.4	8.1	−36.4	−47.4	−42.4	−27.2	−46.0	−14.9
R-B3LYP	29.4	14.2	−14.9	−31.6	−24.0	−11.5	−29.4	−0.6
UHF	22.0	−6.5	12.9	−24.8	−1.0	1.2	−1.0	2.7
U5050	56.4	(a)	1.8	−10.7	−0.6	2.4	−0.8	5.1
UB3LYP	(a)	(a)	2.4	−6.72	−0.2	3.4	−0.6	7.1
SF-CIS	23.1	8.5	5.9	−7.3	−1.1	2.8	−1.3	5.8
SF-B3LYP	53.9	n.a.	12.8	−6.8	3.8	15.1	n.a.	22.7
SF-5050	41.7	22.3	3.5	−10.6	−0.2	6.8	−1.13	12.6
Theor.	37.6 [b]	19.3 [b]	3.9 [b]	−10.0 [c]	−0.7 [d]	4.8 [d]	−1.35 [e]	9.8 [f]
Expt.	37.5±0.3 [g]	21.0±0.3 [g]	3.8±0.3 [g]	<0 [h]				

[a]No lower unrestricted singlet solution could be found.
[b]Reference 14.
[c]Reference 69.
[d]Reference 70.
[e]Reference 71.
[f]Reference 72.
[g]Reference 67.
[h]Reference 68.

mental values,[91] restricted and unrestricted HF and CCSD(T), and unrestricted B3LYP results[76] are also tabulated for comparison. Note that the usually reliable CCSD(T) method fails to improve RHF results and yield very large imaginary frequencies for ω_{10} and ω_{18}. Unrestricted HF, B3LYP, and CCSD(T) do not yield imaginary frequencies. For seven experimentally measured frequencies, the agreement between U-CCSD(T) and the experiment is good. Moreover, U-B3LYP frequencies are very close to U-CCSD(T). Both SF-B3LYP and SF-5050 yield real frequencies for these two problematic modes. Moreover, SF-5050 frequencies are following closely the U-CCSD(T) numbers. For the seven measured frequencies, the SF-5050 frequencies are all slightly higher than experimental values (which is not surprising since no anharmonicity corrections have been included). Some of the SF-B3LYP frequencies

TABLE IV. Harmonic vibrational frequencies (cm^{-1}) for the ground ^1A_g state of *p*-benzyne, 6-31G** basis set.

Mode	RHF[a]	UHF[a]	U-B3LYP[a]	R-CCSD(T)[a]	U-CCSD(T)[a]	SF-B3LYP	SF-5050	Expt.[b]
ω_1 (a_g)	3414	3370		3264	3258	3220	3317	
ω_2 (a_g)	1379	1538		1342	1498	1269	1440	
ω_3 (a_g)	1256	1194		1174	1183	1170	1202	
ω_4 (a_g)	980	993		1018	1044	964	1065	
ω_5 (a_g)	775	630		608	620	705	660	
ω_6 (a_u)	1004	965		913	938	896	994	
ω_7 (a_u)	489	390		417	407	442	450	
ω_8 (b_{1g})	961*i*	806		349	771	337	722	
ω_9 (b_{2g})	946	943		832	897	865	961	
ω_{10} (b_{2g})	310*i*	673		5612*i*	577	493	616	
ω_{11} (b_{3g})	3396	3353		3250	3242	3205	3302	
ω_{12} (b_{3g})	1869	1624		1657	1683	1697	1738	
ω_{13} (b_{3g})	1335	1369		1301	1309	1248	1327	
ω_{14} (b_{3g})	592	625		586	584	552	597	
ω_{15} (b_{1u})	3391	3353		3238	3241	3200	3300	
ω_{16} (b_{1u})	1504	1559	1458	1482	1489	1402	1511	1403
ω_{17} (b_{1u})	1164	1074	1054	1058	1067	1081	1101	976
ω_{18} (b_{1u})	621*i*	1024	940	3739*i*	953	669	973	918
ω_{19} (b_{2u})	3415	3368		3263	3257	3221	3316	
ω_{20} (b_{2u})	1546	1411	1403	1388	1391	1477	1448	1331
ω_{21} (b_{2u})	1144	1388	1256	1275	1256	1107	1254	1207
ω_{22} (b_{2u})	306	1117		1068	1079	864	1076	
ω_{23} (b_{3u})	812	786	757	750	766	738	796	721
ω_{24} (b_{3u})	519	443	445	443	439	463	477	435

[a]Reference 76.
[b]Reference 91.

seem to be closer to the experimental values, however, for ω_{18} SF-B3LYP yields 669 cm^{-1} which is too low as compared with the experimental value of 918 cm^{-1}. This is similar to the ethylene example, where SF-B3LYP torsional potential is too flat around the barrier. Thus, the SF-5050 potential energy surfaces are more accurate than the SF-B3LYP ones.

IV. CONCLUSIONS

We have presented a simple extension of DFT to describe bond-breaking and diradicals. The method describes target multiconfigurational states as spin–flipping excitations from a single-configurational high-spin triplet reference. The resulting equations are identical to the TDDFT/TDA equations, however, they are solved in a subspace of the spin–flipping (e.g., $M_s=-1$) excitations. Similarly to DFT and TDDFT, the SF-DFT model is formally exact (*though not the* TDA) and therefore will yield exact answers with the exact density functional. With the available inexact functionals, SF-TDDFT/TDA represents an improvement over its non-SF counterparts. So far, the best performance has been achieved with the 50/50 functional (50% Hartree–Fock+8% Slater +42% Becke for exchange and 19% VWN+81% LYP for correlation). The SF-DFT/5050 model has been shown to yield accurate equilibrium properties and singlet–triplet energy gaps in medium-sized diradicals, although some troubling failures for small molecules were observed.

ACKNOWLEDGMENTS

A.I.K. acknowledges support from the National Science Foundation CAREER Award (Grant No. CHE-0094116), the Camille and Henry Dreyfus New Faculty Awards Program, WISE Research Fund (USC), and the Donors of the Petroleum Research Fund, administered by the American Chemical Society (PRF-AC grant). Y.S. and M.H.G. acknowledge support from the Director, Office of Energy Research, Office of Basic Energy Sciences, Chemical Sciences Division of the U.S. Department of Energy, under Contract No. DE-AC03-765F00098. Y.S. thanks Lyudmila V. Slipchenko, Sergey V. Levchenko, Dr. Troy van Voorhis, and Prof. Steven R. Gwaltney for helpful discussions. M.H.G. is on appointment as a Miller Research Professor in the Miller Institute for Basic Research in Science.

[1] T. Helgaker, P. Jørgensen, and J. Olsen, *Molecular Electronic Structure Theory* (Wiley, New York, 2000).
[2] B. O. Roos, P. R. Taylor, and P. E. M. Siegbahn, Chem. Phys. **48**, 157 (1980).
[3] M. W. Schmidt and M. S. Gordon, Annu. Rev. Phys. Chem. **49**, 233 (1998).
[4] *Recent Advances in Multireference Methods*, edited by K. Hirao (World Scientific, Singapore, 1999).
[5] A. I. Krylov, C. D. Sherrill, E. F. C. Byrd, and M. Head-Gordon, J. Chem. Phys. **109**, 10669 (1998).
[6] S. R. Gwaltney, C. D. Sherrill, M. Head-Gordon, and A. I. Krylov, J. Chem. Phys. **113**, 3548 (2000).
[7] A. I. Krylov, C. D. Sherrill, and M. Head-Gordon, J. Chem. Phys. **113**, 6509 (2000).
[8] T. van Voorhis and M. Head-Gordon, Chem. Phys. Lett. **330**, 585 (2000).
[9] S. R. Gwaltney, E. F. C. Byrd, T. van Voorhis, and M. Head-Gordon, Chem. Phys. Lett. **353**, 359 (2002).
[10] M. Wladyslawski and M. Nooijen, "The photoelectron spectrum of the NO_3 radical revisited: A theoretical investigation of potential energy surfaces and conical intersections," in ACS Conference Proceedings, 2001 (in press).
[11] A. I. Krylov, Chem. Phys. Lett. **338**, 375 (2001).
[12] A. I. Krylov, Chem. Phys. Lett. **350**, 522 (2001).
[13] A. I. Krylov and C.D. Sherrill, J. Chem. Phys. **116**, 3194 (2002).
[14] L. V. Slipchenko and A.I. Krylov, J. Chem. Phys. **117**, 3694 (2002).
[15] L. Salem and C. Rowland, Angew. Chem. Int. Ed. Engl. **11**, 92 (1972).
[16] P. Hohenberg and W. Kohn, Phys. Rev. **136**, B864 (1964).
[17] W. Kohn and L. J. Sham, Phys. Rev. **140**, A1133 (1965).
[18] R. G. Parr and W. Yang, *Density-functional Theory of Atoms and Molecules* (Oxford University Press, New York, 1989).
[19] E. Runge and E. K. U. Gross, Phys. Rev. Lett. **52**, 997 (1984).
[20] M. Petersilka, U. J. Grossman, and E. K. U. Gross, Phys. Rev. Lett. **76**, 1212 (1996).
[21] M. E. Casida, *Time-Dependent Density Functional Response Theory for Molecules* (World Scientific, Singapore, 1995), Chap. 5.
[22] R. Bauernschmitt and R. Ahlrichs, Chem. Phys. Lett. **256**, 454 (1996).
[23] R. Bauernschmitt, M. Häser, O. Treutler, and R. Ahlrichs, Chem. Phys. Lett. **264**, 573 (1997).
[24] S. Hirata and M. Head-Gordon, Chem. Phys. Lett. **302**, 375 (1999).
[25] S. Hirata and M. Head-Gordon, Chem. Phys. Lett. **314**, 291 (1999).
[26] J. C. Slater, *Quantum Theory of Molecules and Solids: Vol. 4: The Self-Consistent Field for Molecules and Solids* (McGraw–Hill, New York, 1974).
[27] S. H. Vosko, L. Wilk, and M. Nusair, Can. J. Phys. **58**, 1200 (1980).
[28] J. P. Perdew, Phys. Rev. B **33**, 8822 (1986).
[29] A. D. Becke, Phys. Rev. A **38**, 3098 (1988).
[30] C. Lee, W. Yang, and R. G. Parr, Phys. Rev. B **37**, 785 (1988).
[31] J. P. Perdew, J. A. Chevary, S. H. Vosko, K. A. Jackson, M. R. Pederson, D. J. Singh, and C. Fiolhais, Phys. Rev. B **46**, 6671 (1992).
[32] A. D. Becke, J. Chem. Phys. **98**, 5648 (1993).
[33] N. C. Handy and A. J. Cohen, J. Chem. Phys. **116**, 5411 (2002).
[34] J. Gräfenstein, E. Kraka, and D. Cremer, Phys. Chem. Chem. Phys. **2**, 2091 (2000).
[35] O. V. Gritsenko, P. R. T. Schipper, and E. J. Bearends, J. Chem. Phys. **107**, 5007 (1997).
[36] D. Cremer, Mol. Phys. **99**, 1899 (2001).
[37] R. Pollet, A. Savin, T. Leininger, and H. Stoll, J. Chem. Phys. **116**, 1250 (2002).
[38] J. M. L. Martin, Mol. Phys. **86**, 1437 (1995).
[39] C. J. Cramer, F. J. Dulles, D. J. Giesen, and J. Almlöf, Chem. Phys. Lett. **245**, 165 (1995).
[40] J. Gräfenstein, E. Kraka, and D. Cremer, Chem. Phys. Lett. **288**, 593 (1998).
[41] E. K. U. Gross, L. N. Oliveira, and W. Kohn, Phys. Rev. A **37**, 2809 (1988).
[42] M. Filatov and S. Shaik, J. Phys. Chem. A **104**, 6628 (2000).
[43] S. P. de Visser, M. Filatov, and S. Shaik, Phys. Chem. Chem. Phys. **2**, 5046 (2000).
[44] B. I. Dunlap and W. N. Mei, J. Chem. Phys. **78**, 4997 (1983).
[45] F. W. Averill and G. S. Painter, Phys. Rev. B **46**, 2498 (1992).
[46] S. G. Wang and W. H. E. Schwarz, J. Chem. Phys. **105**, 4641 (1996).
[47] E. Kraka, Chem. Phys. **61**, 149 (1992).
[48] J. Gräfenstein and D. Cremer, Chem. Phys. Lett. **316**, 569 (2000).
[49] N. O. J. Malcolm and J. J. W. McDouall, J. Phys. Chem. **100**, 10131 (1996).
[50] T. Leininger, H. Stoll, H.-J. Werner, and A. Savin, Chem. Phys. Lett. **275**, 151 (1997).
[51] B. Miehlich, H. Stoll, and A. Savin, Mol. Phys. **91**, 527 (1997).
[52] P. Borovski, K. D. Jordan, J. Nichols, and P. Nachtigall, Theor. Chim. Acta **99**, 135 (1998).
[53] S. Grimme and M. Waletzke, J. Chem. Phys. **111**, 5645 (1999).
[54] A. J. Sodt, T. van Voorhis, and M. Head-Gordon (unpublished).
[55] I. Tamm, J. Phys. (Moscow) **9**, 449 (1945).
[56] S. V. Levchenko and A. I. Krylov, J. Chem. Phys. **115**, 7485 (2001).
[57] W. Kohn, A. D. Becke, and R. G. Parr, J. Phys. Chem. **100**, 12974 (1996).
[58] J. Kong, C. A. White, A. I. Krylov *et al.*, J. Phys. Chem. **21**, 1532 (2000).
[59] T. H. Dunning, J. Chem. Phys. **53**, 2823 (1970).
[60] P. C. Hariharan and J. A. Pople, Theor. Chim. Acta **28**, 213 (1973).
[61] A. I. Krylov, J. Chem. Phys. **113**, 6052 (2000).
[62] N. Turro, *Modern Molecular Photochemistry* (Benjamin/Cummings, New York, 1978).
[63] *Diradicals*, edited by W. T. Borden (Wiley, New York, 1982).

[64] V. Bonačić-Koutecký, J. Koutecký, and J. Michl, Angew. Chem. Int. Ed. Engl. **26**, 170 (1987).
[65] *Kinetics and Spectroscopy of Carbenes and Biradicals*, edited by M. S. Platz (Plenum, New York, 1990).
[66] K. B. Eisenthal, R. A. Moss, and N. J. Turro, Science **225**, 1439 (1984).
[67] P. G. Wenthold, R. G. Squires, and W. C. Lineberger, J. Am. Chem. Soc. **120**, 5279 (1998).
[68] B. B. Wright and M. S. Platz, J. Am. Chem. Soc. **105**, 628 (1983).
[69] S. Kato, K. Morokuma, D. Feller, E. R. Davidson, and W. T. Borden, J. Am. Chem. Soc. **105**, 1791 (1983).
[70] A. Skancke, D. A. Hrovat, and W. T. Borden, J. Am. Chem. Soc. **120**, 7079 (1998).
[71] C. D. Sherrill, E. T. Seidl, and H. F. Schaefer III, J. Phys. Chem. **96**, 3712 (1992).
[72] J. D. Xu, D. A. Hrovat, and W. T. Borden, J. Am. Chem. Soc. **116**, 5425 (1994).
[73] E. Kraka and D. Cremer, Chem. Phys. Lett. **216**, 333 (1993).
[74] E. Kraka and D. Cremer, J. Am. Chem. Soc. **116**, 4929 (1994).
[75] E. Kraka, D. Cremer, G. Bucher, H. Wandel, and W. Sander, Chem. Phys. Lett. **268**, 313 (1997).
[76] T. D. Crawford, E. Kraka, J. F. Stanton, and D. Cremer, J. Chem. Phys. **114**, 10638 (2001).
[77] E. Kraka, J. Anglada, A. Hjerpe, M. Filatov, and D. Cremer, Chem. Phys. Lett. **348**, 115 (2001).
[78] C. F. Logan and P. Chen, J. Am. Chem. Soc. **118**, 2113 (1996).
[79] M. J. Schottelius and P. Chen, J. Am. Chem. Soc. **118**, 4896 (1996).
[80] J. Hoffner, M. J. Schottelius, D. Feichtinger, and P. Chen, J. Am. Chem. Soc. **120**, 376 (1998).
[81] C. J. Cramer, J. J. Nash, and R. R. Squires, Chem. Phys. Lett. **277**, 311 (1997).
[82] H. Jiao, P. von R. Schleyer, B. R. Beno, K. N. Houk, and R. Warmuth, Angew. Chem. Int. Ed. Engl. **36**, 2761 (1997).
[83] P. R. Schreiner, J. Am. Chem. Soc. **120**, 4184 (1998).
[84] P. R. Schreiner, J. Am. Chem. Soc. **121**, 8615 (1999).
[85] L. V. Moskaleva, L. K. Madden, and M. C. Lin, Phys. Chem. Chem. Phys. **1**, 3967 (1999)
[86] R. Lindh, A. Bernhardsson, and M. Schütz, J. Phys. Chem. A **103**, 9913 (1999).
[87] B. A. Hess, Jr., Chem. Phys. Lett. **35**, 75 (352).
[88] W. Sander, Acc. Chem. Res. **32**, 669 (1999).
[89] S. L. Buchwalter and G. L. Closs, J. Am. Chem. Soc. **97**, 3857 (1975).
[90] S. L. Buchwalter and G. L. Closs, J. Am. Chem. Soc. **101**, 4688 (1979).
[91] R. Marquardt, A. Balster, W. Sander, E. Kraka, D. Cremer, and J. G. Radziszewiski, Angew. Chem. Int. Ed. Engl. **37**, 955 (1998).